ACS APPLIED MATERIALS & INTERFACES

Research Article

www.acsami.org

Thermo-triggered Drug Release from Actively Targeting Polymer Micelles

Xing Guo,[†] Dan Li,[†] Guang Yang,[†] Chunli Shi,[‡] Zhaomin Tang,[†] Jie Wang,[†] and Shaobing Zhou*[,†,‡]

[†]Key Laboratory of Advanced Technologies of Materials, Ministry of Education, School of Materials Science and Engineering, Southwest Jiaotong University, Chengdu 610031, China

[‡]School of Life Science and Engineering, Southwest Jiaotong University, Chengdu 610031, China

Supporting Information

ABSTRACT: How to deliver the drug to the target area at the right time and at the right concentration is still a challenge in cancer therapy. In this study, we present a facile strategy to control drug release by precisely controlling the thermosensitivity of the nanocarriers to the variation of environmental temperature. One type of thermoresponsive Pluronic F127-poly(D,L-lactic acid) (F127-PLA, abbreviated as FP) copolymer micelles was developed and decorated with folate (FA) for active targeting. FP100 micelles assembled from FP with PLA segment having polymerization degree of 100 had a low critical solution temperature of 39.2 °C close to body temperature. At 37 °C, little amount of encapsulated anticancer drug DOX is released from the FP100 micelles, while at a slightly elevated temperature (40 °C), the shrinkage of thermoresponsive segments causes a rapid release of DOX and instantly increases the drug concentration locally. The cytocompatibility analysis and cellular uptake efficiency were characterized with the fibroblast cell line NIH 3T3 and human cervix adenocarcinoma cell line HeLa. The results demonstrate that this copolymer has excellent cytocompatibility, and FA-decorated FP100 micelles present much better efficiency of cellular uptake and higher cytotoxicity to folate receptor (FR)-overexpressed HeLa cells. In particular, under hyperthermia (40 °C) the cytotoxicity of DOX-loaded FA-FP100 micelles against HeLa cells was significantly more obvious than that upon normothermia (37 °C). Therefore, these temperature-responsive micelles have great potential as a drug vehicle for cancer therapy.

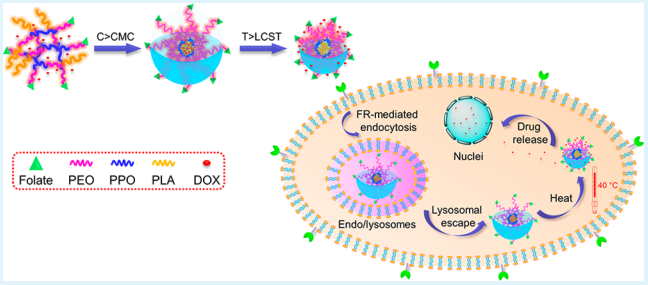

KEYWORDS: *nanotechnology, polymeric micelle, active targeting, thermoresponsive, drug delivery, anticancer*

INTRODUCTION

In the past decade, nanotechnology-based drug delivery system has shown promising results in cancer therapy due to their improved pharmacokinetics and pharmacodynamics via the enhanced permeation and retention (EPR) effect.[1,2] However, the EPR effect does have several limitations, including poor cellular internalization and inefficient intracellular drug release.[3] To overcome these limitations, two promising strategies are primed: one is to construct an actively targeted drug delivery system and the other is to endow a system stimuli-responsibility for controlled drug release.

The active targeting strategy utilizing various targeting ligands that bind to specific proteins overexpressed on cancer cells has provided an opportunity to selectively deliver drugs to the tumor cells via receptor-mediated endocytosis.[4] For instance, folate (FA), a low-molecular-weight vitamin, binding with high affinity to the folate receptor (FR), a membrane-anchored protein,[5] has been widely used to modify nanocarriers to further improve the passive targeting systems and accumulate drugs in cancer cells by FR-mediated endocytosis.[6−9] Although the active targeting system can significantly facilitate the cell internalization by receptor-mediated endocytosis, the intracellular drug release cannot be still realized and in turn the high therapeutic efficiency of encapsulated agent to solid tumors cannot be exerted after the cell internalization if these nanocarriers lack enough responsiveness to the tumor extracellular and/or intracellular microenvironment.

To address this challenge, the stimuli-responsive delivery systems have been extensively developed. Generally, these systems can be classified into two classes: exogenous stimuli-responsive and endogenous stimuli-responsive drug delivery systems.[10] Externally applied stimuli include temperature changes,[11,12] magnetic fields,[13,14] ultrasounds,[15] light,[16,17] and electric fields;[18] intrinsic stimuli include variations in pH,[19,20] redox potential,[21,22] or the concentrations of enzymes.[23,24] Of these stimuli, temperature is a frequently investigated responsive strategy. On the one hand, tumor tissues possess abnormal temperature gradients as compared with those of normal ones;[25,26] on the other hand, tumor tissues are much more sensitive to high temperatures. Therefore, effectively killing of tumor by hyperthermia can occur in the range 40−43 °C.[27] A variety of thermoresponsive drug delivery systems were

Received: March 9, 2014
Accepted: April 30, 2014
Published: April 30, 2014

utilized for combining hyperthermia with chemotherapy.[28,29] One of the widely investigated thermoresponsive polymers is Pluronic F127 composed of poly(ethylene oxide)−poly(propylene oxide)−poly(ethylene oxide) (PEO−PPO−PEO), which plays a key role in controlling drug release because of its outstanding thermal response. However, the unacceptably high critical micellization concentration (CMC) and low lower critical solution temperature (LCST) of Pluronic F127 due to the weak hydrophobic PPO block limit the potential applications as drug delivery systems. To solve this problem, modification of hydrophobic polyester blocks on Pluronic F127 can be regarded as a good way, which cannot only increase the stability and LCST of Pluronic F127 but also endow the copolymer biocompatibility as well as biodegradability. F127 has been reported for developing a thermal-triggered "on−off" nanocarrier by decreasing temperature (also called cold shock or cryotherapy).[30,31] In this case, drug release occurs as a consequence of cooling; however, the manipulation of this cryotherapy is not convenient for clinical application compared with hyperthermia.

Accordingly, in this study, we present a thermoresponsive drug delivery system with active targeting capacity based on Pluronic F127-poly(D,L-lactic acid) (FP) copolymer decorated with FA ligands. As shown in Scheme 1, this amphiphilic copolymer can self-assemble into micelles in aqueous solution, and the micelles can be specifically taken up by FR-overexpressed tumor cells through receptor-mediated endocytosis, and subsequently rapidly release the payloads inside cells at low hyperthermia (40 °C). The thermoresponsive behaviors, active targeting ability, intracellular drug release, and in vitro antitumor effect both at 37 and 40 °C were systematically evaluated.

Scheme 1. Schematic Representation of Thermosensitive Nanocarrier Working as a Targeted Drug Delivery System with Controlled Drug Release[a]

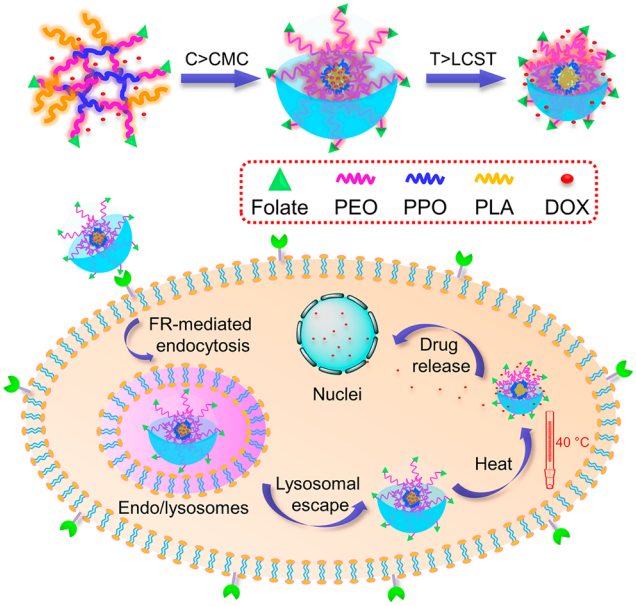

[a]Micelle formation occurs if the concentration of polymer is greater than CMC. Above the LCST the thermosensitive block shrank, inducing the release of incorporated agents. The nanocarrier can target tumor cells overexpressing folate receptor, and rapidly intracellular drug release will be triggered by heating (40 °C) upon LCST on the tumor tissue.

EXPERIMENTAL SECTION

Materials. Pluronic F127 (M_n 12600) was purchased from Aldrich (USA). D,L-lactide was synthesized in our laboratory. Folate (FA) was purchased from Chengdu KeLong Chemical Reagent Company (Sichuan, China). Doxorubicin hydrochloride (DOX·HCl) was purchased from Zhejiang Hisun Pharmaceutical Co., Ltd. (China). Hoechst 33342 and LysoTracker Green were purchased from Beyotime Biotechnology Co. Ltd. (Nantong, China). All the other chemicals were purchased from commercial supplier and used as received.

Cell Culture. The mouse fibroblast cell line NIH 3T3, human cervix adenocarcinoma cell line HeLa and human lung epithelial carcinoma cell line A549, were obtained from Sichuan University (China). Cells were cultured in RPMI 1640 medium containing 10% FBS at 37 °C in 5% CO_2 in a humidified atmosphere.

Synthesis of F127-PLA Copolymers (FP). F127-PLA copolymers were synthesized through ring-opening polymerization of D,L-lactide initiated by Pluronic F127 using $Sn(Oct)_2$ as catalyst.[32] By varying the mole ratio of reactants used in the polymerization, the PLA to F127 molecular weight ratio of the copolymer was controlled. Taken FP100 as example, Pluronic F127 (2.52 g, 0.2 mmol), D,L-lactide (1.44 g, 10 mmol) and $Sn(Oct)_2$ (0.1 wt % of D,L-lactide) were quickly added to a round-bottom flask with a stopcock, which was preheated to remove the moisture. The mixture was degassed under vacuum and then heated to 150 °C for 4 h of reaction. After that, the content was cooled to room temperature. The product was dissolved in dichloromethane, precipitated in excess cold ethanol, and collected by centrifugation. The copolymers were dried overnight under vacuum.

Synthesis of CDI-Activated F127 (CDI-F127-OH). CDI-F127-OH was synthesized by a modified procedure as described earlier.[33] Briefly, *N,N′*-Carbonyldiimidazole (CDI) (0.16 g, 1 mmol) and Pluronic F127 (12.6 g, 1 mmol) were respectively dissolved in dry dichloromethane. The solution of CDI was added dropwise into the Pluronic F127 solution at room temperature in 2 h under nitrogen atmosphere. The mixture was kept stirring for another 4 h. The excess dichloromethane was removed by rotary evaporator. The product was precipitated in ethyl ether for three times to remove unreacted CDI. The CDI-F127-OH was dried under vacuum to obtain the white powder (yield: 92.4%).

Synthesis of CDI-F127-PLA Copolymer (CDI-FP). The CDI-F127-PLA copolymer was synthesized as mentioned earlier. For instance, CDI-FP100 was synthesized as follows. CDI-F127-OH (10.16 g, 0.8 mmol), D,L-lactide (5.76 g, 40 mmol) and $Sn(Oct)_2$ (0.1 wt % of D,L-lactide) were reacted at 150 °C for 4 h. Afterward, the product was dissolved in dichloromethane and precipitated in ethanol, and collected by centrifugation. The CDI-FP100 copolymer was dried overnight under vacuum (yield: 71.2%).

Synthesis of Amino-Terminated F127-PLA Copolymer (NH_2−FP). Taken NH_2−FP100 as example, the CDI-FP100 (9.95 g, 0.5 mmol) was dissolved in dry dichloromethane and added dropwise to 5 mL of 1,2-ethylenediamine at room temperature in 2 h. The mixture was kept stirring overnight. The unreacted 1,2-ethylenediamine and excess dichloromethane were removed by rotary evaporator. The product was precipitated in excess cold ethanol and collected by centrifugation. The NH_2−FP100 was dried under vacuum to obtain the light yellow powder (yield: 75.1%).[34]

Synthesis of Folate-conjugated F127-PLA Copolymer (FA-FP). Folate (0.13 g, 0.3 mmol), NHS (0.03 g, 0.3 mmol), and EDC·HCl (0.06 g, 0.33 mmol) were dissolved in 100 mL DMSO. The mixture was stirred at room temperature under nitrogen atmosphere in the dark overnight. Then, NH_2−FP100 (5.96 g, 0.3 mmol) and several drop of triethylamine were added, and the mixture was reacted for another 24 h. DMSO and unreacted folate were removed by dialysis against deionized water for 3 days. FA-FP100 was collected by lyophilization (yield: 83.9%).[35]

Characterizations of Copolymer. Fourier transform infrared (FT-IR) spectra were carried out using a Nicolet 5700 spectrometer in the range between 4000 and 500 cm^{-1}. KBr tablets were prepared by grinding the sample with KBr and compressing the whole into a transparent tablet. ^1H NMR spectra was obtained on a Bruker AM 300 apparatus. $CDCl_3$ or DMSO-d_6 was used as a solvent. Chemical shifts are expressed in parts permillion, ppm (δ). Gel permeation chromatography (GPC) was performed with a Water 2695 pump and a Styragel HT4DMF column calibrated with polystyrene standards operated at 40 °C and series 2414 refractive index detector. UV−vis spectrophotometer (UV-2550, Shimadzu, Japan) was employed to confirm the graft of folate to NH_2−FP and quantify the grafted amount.

Preparation of Polymeric Micelles. The blank micelles were prepared by a solvent evaporation method. Briefly, FP or FA-FP copolymer was dissolved in 5 mL of tetrahydrofuran as a good solvent; the solution was then added dropwise to 10 mL of deionized water as a selective solvent under high-speed stirring. The polymeric micelles were fabricated after the complete evaporation of tetrahydrofuran. The method of preparing the DOX-loaded micelles was similar to mentioned above. The only difference is that DOX·HCl was first dissolved in tetrahydrofuran, and several drops of triethylamine was added to remove hydrochloric acid of DOX·HCl. After that, the copolymer was added to the solution of DOX, the mixture was then added dropwise to deionized water. After tetrahydrofuran was evaporated completely, the DOX-loaded micelles were transferred into dialysis bag (MWCO 1000) against deionized water to remove the unloaded DOX.

Characterizations of Micelles. Fluorescence spectrometer (F-7000, Hitach, Japan) was performed to determine the critical micelle concentration (CMC) values of FP copolymers. Pyrene was used as a fluorescent probe. The excitation wavelength was set to 333 or 339 nm, and the fluorescence intensity was detected at 372 nm. The intensity ratio of peaks excited at 339 nm to those at 333 nm was plotted against the logarithm of concentration to measure CMC.

Dynamic light scattering (DLS) (ZETA-SIZER, MALVERN Nano-ZS90, Malvern, Ltd., U.K.) was employed to examine the average size of micelles. Each measurement was carried out in triplicate and an average value was reported.

A transmission electron microscopy (TEM) instrument equipped with a JEOL 2010F instrument (JEOL Ltd., Japan) operated at 200 kV was employed to discern the morphologies of micelles. Samples were prepared by dipping a drop of the micellar solution (1 mg/mL) on a copper grid and dried in air; then, a drop of phosphotungstic acid solution (1% w/w) was added to the copper grid to stain the micelles. Afterward, a filter paper was used to absorb the phosphotungstic acid solution. The grid was completely dried before TEM observation.

DOX-loading content (LC) and encapsulation efficiency (EE) were detected by UV−vis. The DOX-loaded micelles were lyophilized before detection. The lyophilized micelle powder was weighed and redissolved in DMSO. The absorbance of DOX at 488 nm was measured to quantify the concentration of DOX in DMSO using a pre-established calibration curve. LC and EE were calculated by eq 1 and 2, respectively.

$$\text{LC}\ (\%) = \frac{\text{weight of the drug in micelles}}{\text{weight of micelles}} \times 100 \quad (1)$$

$$\text{EE}\ (\%) = \frac{\text{weight of the drug in micelles}}{\text{weight of the drug in feed}} \times 100 \quad (2)$$

Thermoresponsive Behaviors. The thermoresponsive properties of FP micelles were investigated by DLS and UV−vis. The experimental temperature range was 25−55 °C. Size and absorbance at λ = 500 nm of micellar solutions (5 mg/mL) were recorded at every 5 °C interval. For each temperature, the solutions were equilibrated for 15 min. LCST was defined as the temperature at 50% absorbance in the curve of the normalized absorbance versus temperature.

The effects of temperature and concentration on aqueous phase behavior of the FP micelles were measured by UV−vis. The experimental temperature was started at 25 °C, and the micellar concentration range is from 1 mg/mL to 10 mg/mL. Absorbance at λ = 500 nm of micellar solutions was recorded at every 0.1 °C interval. The opaque temperature was determined as the onset point of the abrupt increase in the UV absorption, and the precipitate temperature was determined as the temperature when the precipitate of the solution was formed.

In Vitro Drug Release. In vitro drug release was measured by a fluorescence spectrometer. The temperature-dependent release rate of DOX from micelles was first investigated. The DOX-loaded FP freeze-dried powders were suspended in phosphate buffer (PBS) at pH 7.4. The solutions were dialyzed against PBS under a predetermined sink condition. Afterward, the samples were kept at 37 or 40 °C in a thermostated incubator with a shaking speed at 100 cycles/min. The fluorescent intensity of DOX was monitored at selected time intervals from 0.5 to 48 h. The cumulative drug release percentage was calculated based on the emission intensity of DOX at 595 nm.

To further analyze the release of DOX from micelles against both temperature and pH, the DOX fluorescence intensity of drug-loaded micellar solutions was directly measured. The drug-loaded freeze-dried micelle powders were suspended in phosphate buffer (PBS) at pH 7.4 or acetate buffered solution (ABS) at pH 5.0. Then the samples were kept at 37 or 40 °C, the DOX fluorescence intensity was recorded at selected time intervals from 5 to 60 min.

Cytocompatibility Assay. Cytocompatibility of blank micelles was evaluated by Alarmar blue assay and live/dead staining. Alarmar blue assay was performed to quantify the cell viability after treatment. Briefly, 3T3 or HeLa cells were seeded in 48 well plates at an initial density of 2×10^4 cells/well for 24 h prior to treatment. On the following day, HeLa cells were treated with blank micelles with different concentrations ranging from 10 μg/mL to 500 μg/mL, and 3T3 cells were treated with blank micelles in the range from 10 μg/mL to 100 μg/mL. The medium was removed 24 h later and the cells were rinsed three times by PBS. Following treatment, 300 μL of Alamar Blue solution (10% Alamar Blue, 80% media 199 (Gibcos), and 10% FBS, v/v) was added for further 3 h of incubation. The Alamar blue solutions were transferred into a 96-well plate and read by an automated microplate spectrophotometer (ELX800 Biotek, U.S.A.) at 570 nm. Each concentration point was determined from samples from four separate wells. Cell viability was calculated by means of eq 3:

$$\text{cell viability}(\%) = \frac{\text{OD}_{570(\text{sample})} - \text{OD}_{570(\text{blank})}}{\text{OD}_{570(\text{control})} - \text{OD}_{570(\text{blank})}} \times 100 \quad (3)$$

Live/dead staining was employed to directly visualize the survival and apoptosis of cells. In brief, 3T3 or HeLa cells were seeded in 24 well plates at a density of 1×10^4 cells/well for 24 h prior to treatment. The cells were treated with 2 mM calcein acetoxymethylester (Calcein-AM) for 10 min and 4 mM propidium iodide (PI) for 10 min after 24 h of incubation with different concentrations of blank micelles. Live cells were stained green and dead cells were stained red when visualized by fluorescence microscopy.

Cellular Uptake and Subcellular Localization. Fluorescence microscope was used to evaluate the cellular uptake of various formulations. A549 cells without FR expressions were seeded in 6 well plates at a density of 10×10^4 cells/well. The next day, cells were treated with free DOX and DOX-loaded micelles for 3 h of incubation at 37 °C. Then, the cells were rinsed with PBS and fixed with 2.5% glutaraldehyde, and stained with 4′,6-diamidino-2-phenylindole (DAPI). The DAPI fluorescence (blue) and DOX fluorescence (red) in the cells were detected by an inverted fluorescence microscope (Olympus, CKX41).

The subcellular localization was examined by confocal laser scanning microscopy. HeLa cells with high FR expressions were seeded in 6 well plates at a density of 10×10^4 cells/well for 24 h, treated with free DOX and DOX-loaded micelles. After incubation for 3 h at 37 °C, cells were rinsed with PBS, stained with Hoechst 33342 and Lysotracker Green (Beyotime Biotech, China) for cell nuclei and lysosomes, respectively. The treated cells were observed on a confocal microscope (Olympus FV1000). Hoechst 33342, DOX, and

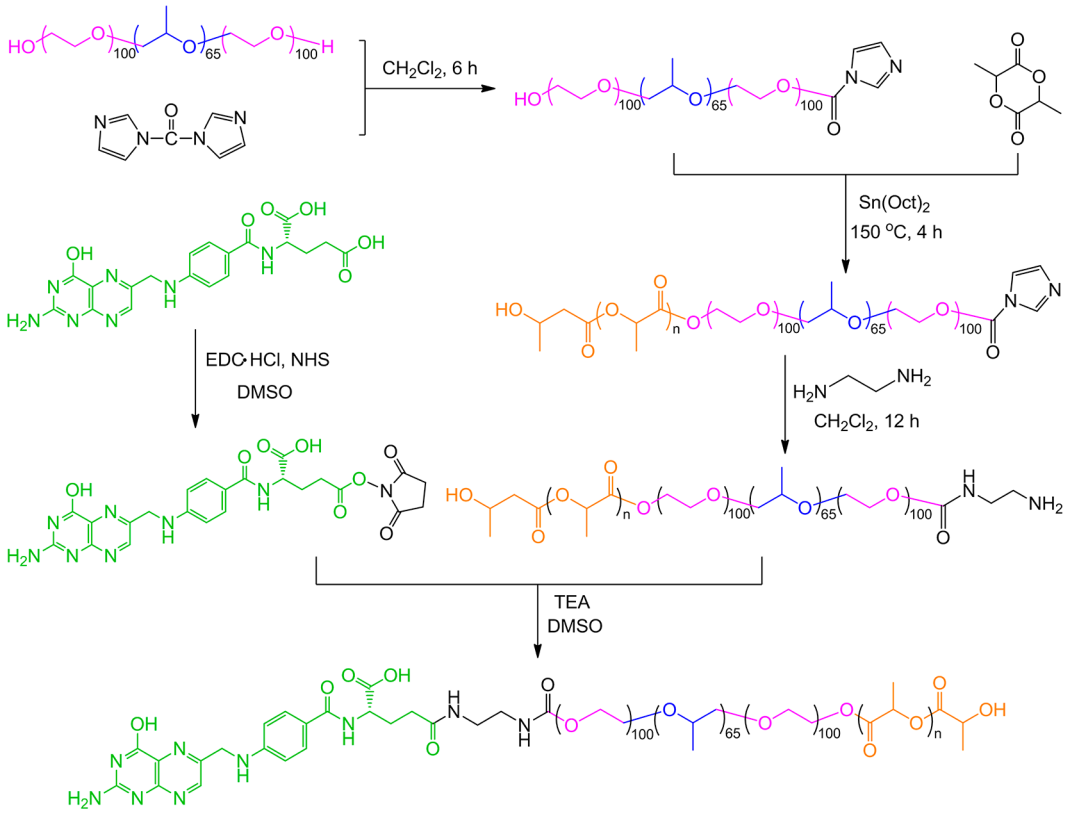

Figure 1. Synthesis of FA-FP copolymer.

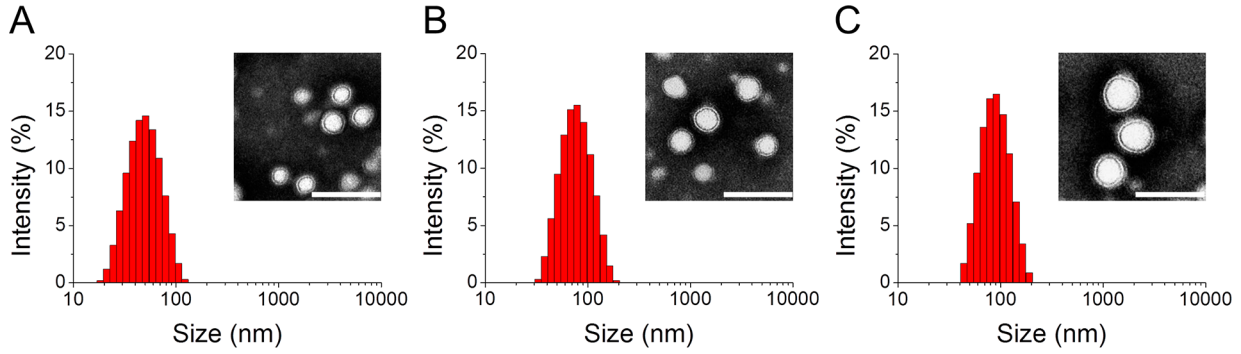

Figure 2. TEM images and dynamic light scattering data for determining the morphology and hydrated particle sizes of FP50 (A), FP100 (B), and FP200 (C), micelles (scale bar =100 nm).

Lysotracker Green were excited at 352, 488, and 504 nm, respectively. The emission wavelengths of Hoechst 33342, DOX, and Lysotracker Green are 455, 595, and 511 nm, respectively.

The quantitative measurements of the cellular uptake of various formulations were made by using flow cytometry. HeLa cells (10×10^4 cells/well) grown in 6-well plates were treated with free DOX and DOX-loaded micelles at 37 °C for 3 h. After being rinsed with PBS, cells were detached with the trypsine-EDTA solution and then resuspended in PBS. Cellular uptake was then analyzed on a FACSCalibur flow cytometer (BD Biosciences, U.S.A.).

Effect of Temperature on Cytotoxicity. The cytotoxicity of the DOX-loaded micelles as a function of temperature was evaluated as well. HeLa cells were incubated with free DOX and DOX-loaded micelles at 37 or 40 °C for 1 h. After incubation at desired temperatures, the cells were incubated at 37 °C for further 23 h. Cytotoxicity was tested by Alarmar blue assay and live/dead staining. IC_{50} values (50% cell inhibition) were calculated.

Cell Apoptosis. For quantitative measurement of apoptosis affected by different temperatures, HeLa cells (10×10^4 cells/well) grown in 6-well plates were treated with free DOX and DOX-loaded micelles at 37 or 40 °C for 1 h. After incubation at desired temperatures, the cells were incubated at 37 °C for further 23 h. After that, the cells were detached with EDTA-free trypsin solution, rinsed twice with PBS and harvested in binding buffer, stained with Annexin V-FITC and PI for 15 min at room temperature in the dark, and then analyzed by FACSCalibur system.

Statistical Analysis. SPSS software was used for the statistical data analysis. Results are expressed as means ± SD with statistical significance of the differences in the cellular uptake determined by flow cytometry between each group were confirmed by a Student's *t*-test. The differences were considered significant for p values * < 0.05.

RESULTS AND DISCUSSION

Synthesis and Characterization of Copolymer. To optimize the temperature responsiveness, FP copolymers with varying compositions were synthesized through ring-opening polymerization as shown in Figure S1 in Supporting

dx.doi.org/10.1021/am501422r | ACS Appl. Mater. Interfaces 2014, 6, 8549−8559

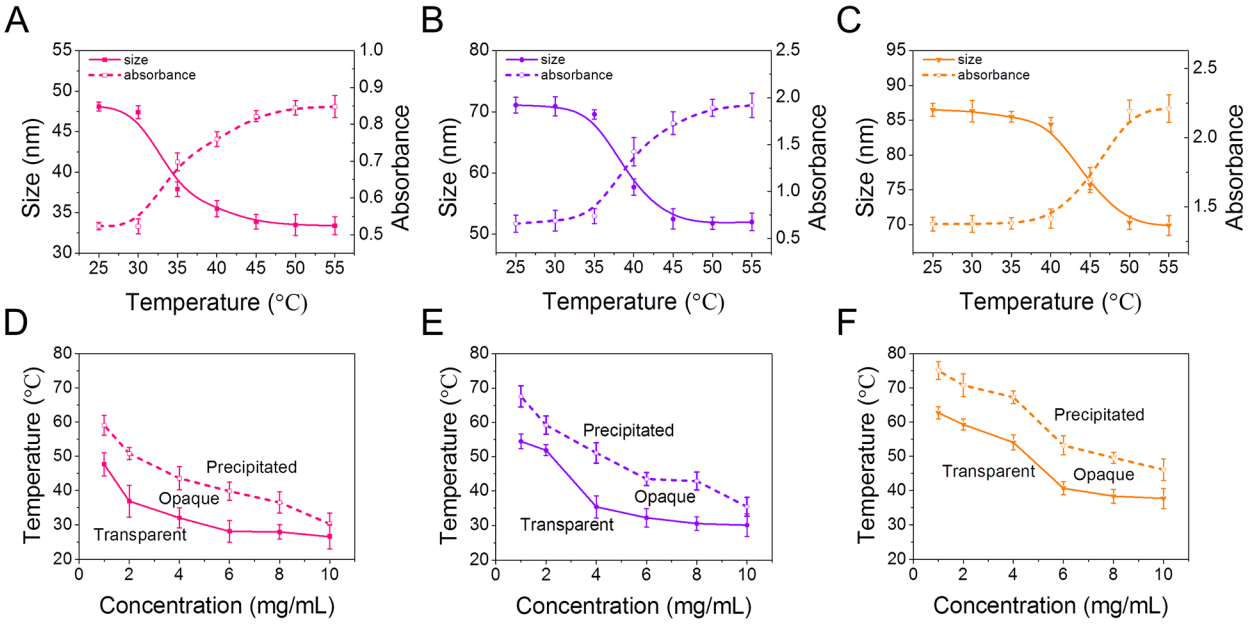

Figure 3. Thermo-responsibility of FP micelles. Size and absorbance changes of FP50 (A), FP100 (B), and FP200 (C) micelles (5 mg/mL) as a function of temperature. The effects of temperature and concentration on aqueous phase behavior of the FP50 (D), FP100 (E), and FP200 (F) micelles. All data are shown as mean ± SD (n = 3).

Information (SI). Three mole ratios of the copolymers were synthesized with F127/PLA of 7:2, 7:4, and 7:8, corresponding to PLA segment with the polymerization degree of 50, 100, and 200, respectively. The chemical structure of the copolymers was confirmed by FT-IR and ^{1}H NMR. The FT-IR spectra of the FP copolymers are represented in Figure S2 in SI. A typically strong stretching band appeared at 1762 cm^{-1}, which is attributed to the C═O stretching vibrations of the ester carbonyl group in PLA segment. The result implied that the copolymers were possibly successfully synthesized. ^{1}H NMR spectroscopy was employed to further confirm the formation of FP copolymers (SI, Figure S3). Besides, the composition of the copolymers was calculated by ^{1}H NMR and the molecular weight and its distribution were determined by GPC; the results are almost in line with the theoretical composition (SI, Table S1). The FA-decorated FP copolymer (FA-FP) for active targeting was further synthesized through several reactions as shown in Figure 1. The chemical structures of the intermediates and end products were confirmed by ^{1}H NMR as well (taken FA-FP100 as example) (SI, Figure S4).

Preparation and Characterization of Micelles. The blank micelles and DOX-loaded micelles were prepared by a solvent evaporation method. The size of the resultant FP micelles was determined by DLS and TEM. The result showed that the size of the micelles increases with an increase in the length of hydrophobic PLA block (SI, Table S2 and Figure 2), which is well consistent with the earlier research.[36] Fluorescence measurements were carried out using pyrene as a fluorescent probe to determine the CMC of FP micelles. It was observed that CMC values decreased with increasing the hydrophobic chain length of the copolymer (SI, Figure S5 and Table S2). Moreover, DOX-loading content (LC) and encapsulation efficiency (EE) of DOX-loaded micelles are summarized in SI, Table S2, as well. The LC and EE depended mainly on the ratio of the hydrophobic and hydrophilic segments.[37] With increasing the ratio of PLA to F127, the LC and EE in micelles increased from 3.82 to 6.23%, and from 42.02 to 68.53%, respectively. This result could be attributed to an increase in size of the hydrophobic core of the micelle.

Thermoresponsive Behaviors. To examine the thermoresponsive behaviors of the FP micelles, we measured the size and absorbance of micellar solutions as a function of temperature. As shown in Figure 3A–C, all three samples exhibit thermoresponsive performance as manifested by the decrease of size and the increase of absorbance when temperature is raised from 25 to 55 °C. The shrinkage of the FP micelles is attributed to the opposing thermal effect between the two polymers,[38] which makes it possible for the micelles to pump the drug out. Interestingly, the original sizes of the FP micelles were obtained again by cooling to 25 °C (SI, Figure S6), this thermo-reversible changes in size indicated that the micellar structure were not disrupted in this temperature ranges. The LCST of FP50, FP100 and FP 200 micelles is 35.6, 39.2, and 45.8 °C, respectively, which shifted to higher temperatures with increasing of PLA block. This result was due to the fact that the longer PLA segment would have a stronger interaction with F127.[38] To trigger drug release in the tumor tissues subjected to low hyperthermia (40 °C), FP100 micelles that possess a LCST just above normothermia is desirable.

The effects of temperature and concentration on aqueous phase behavior of the FP micelles were further investigated. As shown in Figure 3D–F, these micelles showed a transparent-opaque-precipitated transition in response to the elevated temperature from 25 to 80 °C. We can see that the opaque temperature and precipitated temperature decrease with the increase of the micellar concentration. Besides, the F127/PLA proportion also has a great impact on the thermoresponsive transition as the opaque temperature and precipitated temperature shifted to higher temperature when the PLA content in copolymer increased. Therefore, both the F127/PLA proportion and the micellar concentration affect the transition temperature.

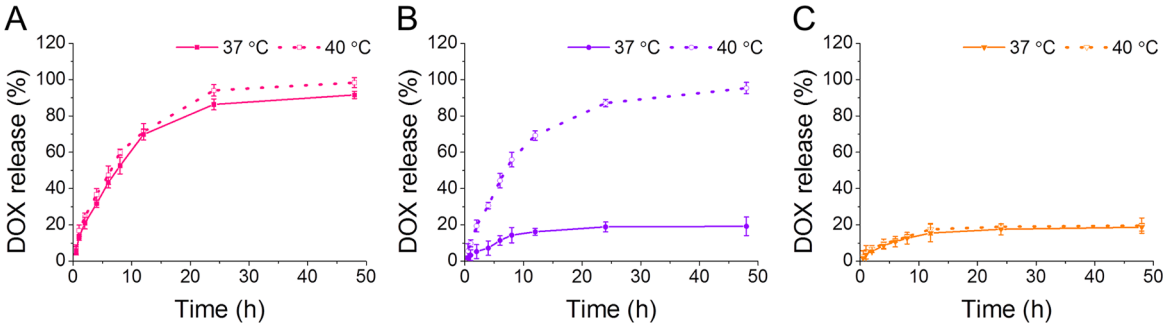

Figure 4. In vitro drug release profiles of DOX-loaded FP50 (A), FP100 (B), and FP200 (C) micelles in PBS solution at pH 7.4 at 37 and 40 °C. Data are shown as mean ± SD (n = 3).

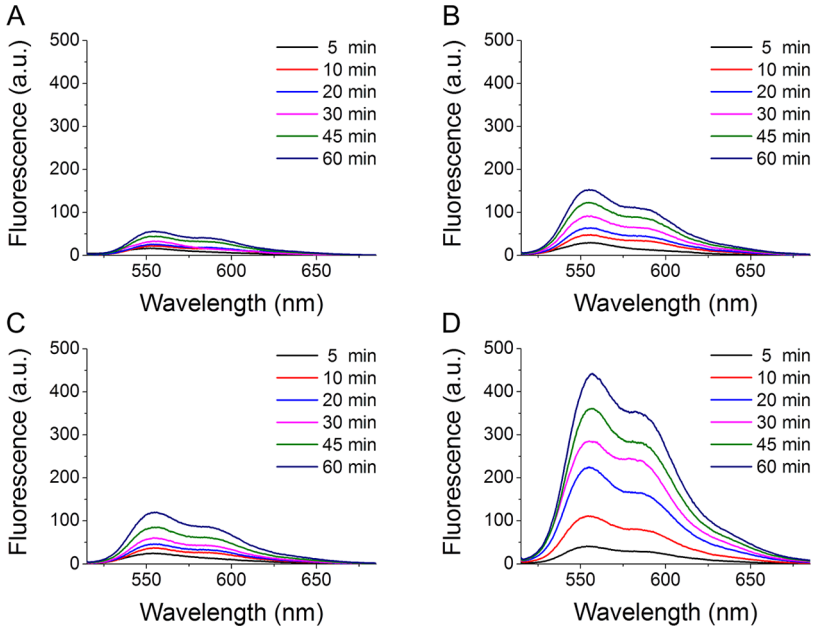

Figure 5. Fluorescence emission spectra of DOX-loaded FP100 micelles under pH 7.4 at 37 °C (A) and 40 °C (B) or under pH 5.0 at 37 °C (C) and 40 °C (D) for 1 h.

In Vitro Drug Release. Figure 4 shows the in vitro release profiles of DOX from the FP micelles at 37 and 40 °C, respectively. DOX release from the FP50 micelles was characterized with a burst followed by a sustained fast release, reaching 91.57% at 37 °C and 98.36% at 40 °C within 48 h (Figure 4A). In contrast, FP100 micelles yielded a much slower release at 37 °C while the same fast release at 40 °C (Figure 4B). The amounts of DOX released from the FP200 micelles were less than 20% during the entire course of the study at both temperatures (Figure 4C). The results indicated that the drug release from the FP micelles was greatly affected by the environmental temperature variation. The core−shell structure of micelles could keep stable when the temperature was below the LCST. Upon heating above the LCST the hydrophilic outer shell collapses and the drug can migrate out of the micelles.[39] Thus, FP50 micelles with a LCST of 35.6 °C are unstable at 37 °C, while FP200 micelles with a LCST of 45.8 °C can still keep the core−shell structure even at 40 °C. Neither the early release of drug during blood circulation nor the incapable drug release in the tumor tissue can achieve the therapeutic effect to solid tumor. Since the FP100 micelles with a LCST between 37 and 40 °C remained stable under normothermia and exhibited rapidly drug release upon low hyperthermia in tumor tissues, these micelles were expected to be the most appropriate candidate to deliver anticancer drug for cancer therapy.

From above discussion, we can know that FP100 micelles possess a highly temperature-dependent drug release profile. Since pH values vary in normal tissues (pH 7.4) and cancer cells (pH 4.5−6.5),[40,41] we further study whether the variation of pH value influences the drug release behavior of these micelles. As shown in Figure 5A, the DOX fluorescence intensity was very weak within 1 h under pH 7.4 at 37 °C, whereas it was obviously intensified when increasing the temperature to 40 °C (Figure 5B) or decreasing the pH to 5.0 (Figure 5C). The release rate at pH 5.0 was much faster than that at pH 7.4, which is mainly attributed to the increased solubility of DOX at acidic pH resulted from the protonation of the glycosidic amine. Furthermore, the sample under pH 5.0 at 40 °C showed the highest DOX fluorescence intensity, indicating the fastest release of DOX among the four groups (Figure 5D). Thus, the FP100 micelles can be triggered to release cargoes by both exogenous low hyperthermia and endogenous lysosomal acidic pH after internalization by tumor cells.

Characterizations of FA-FP100. Due to the optimal thermoresponsive property among the three kind of copoly-

dx.doi.org/10.1021/am501422r | ACS Appl. Mater. Interfaces 2014, 6, 8549−8559

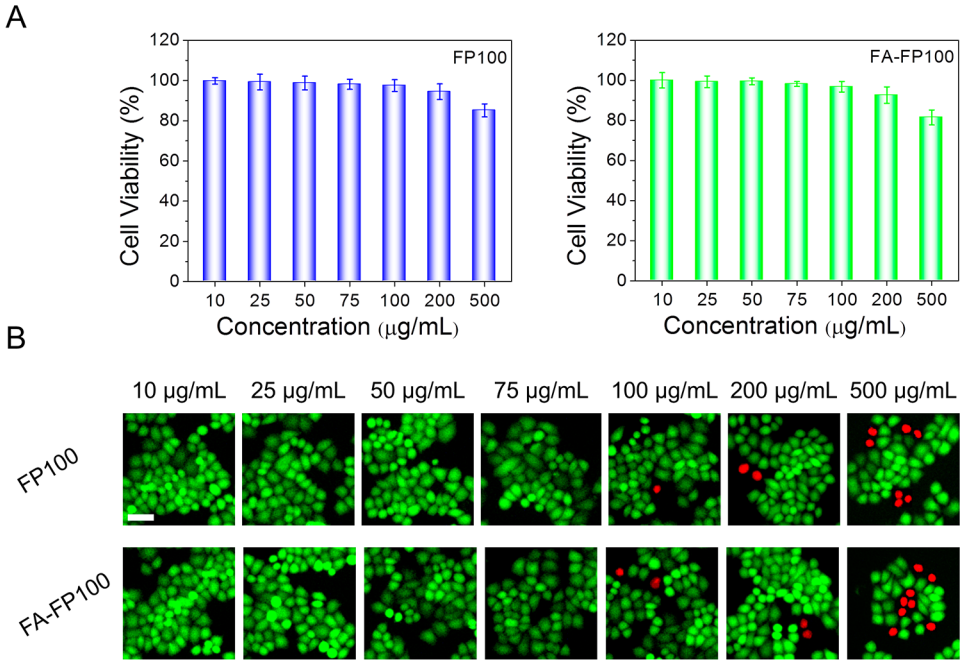

Figure 6. (A) Cell viability of HeLa cells with different concentrations of blank micelles prepared from FP100 and FA-FP100 after 24 h. Data are shown as mean ± SD (n = 4). (B) Fluorescence images showing the viability of HeLa cells following treatment with different concentrations of FP100 and FA-FP100 micelles. Green calcein fluorescence and red PI fluorescence indicating live and dead cells, respectively.

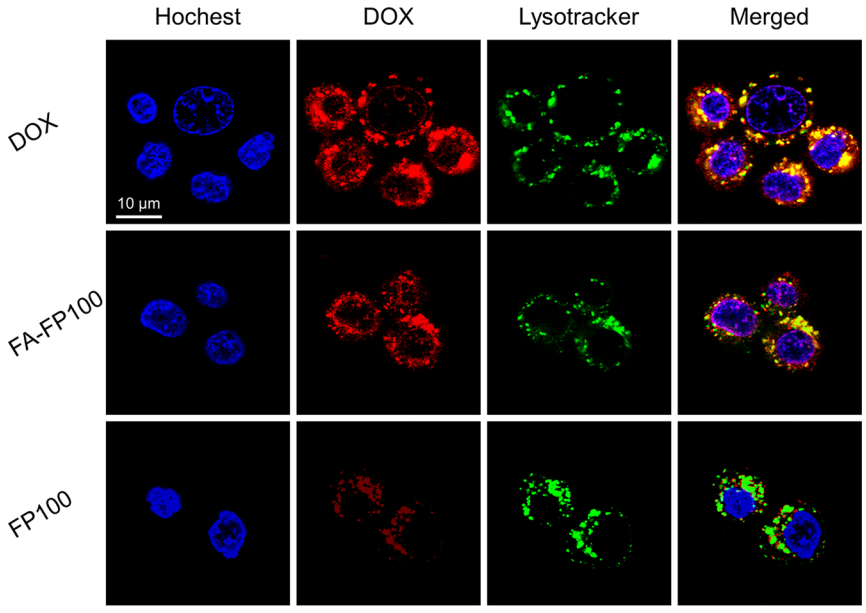

Figure 7. CLSM images of HeLa cells incubated with various DOX formulations for 3 h. All samples have a DOX concentration of 5 μg/mL. The nuclei and lysosomes of the cells were stained with Hoechst 33342 (blue) and Lysotracker (green), respectively.

mers, FP100 was chosen to decorate with folate for the following cell test. UV−vis spectrophotometer was measured to confirm the graft of folate to FP100 and quantify the grafted amount. As can be seen in SI, Figure S7A, two profound UV absorbance peaks around 287 and 363 nm attributed to the aromatic ring of folate occur in FA-FP100, and the grafted amount of folate to FP100 is 72.56% on a molar ratio basis. FA-FP100 micelles were characterized to evaluate if they have thermoresponsiveness similar to FP100 micelles. As shown in SI, Figure S7B, FA-FP100 micelles possessed almost the same size and morphology as compared with FP100 micelles (Figure 2B). Interestingly, FA-FP100 micelles had a LCST of 39.6 °C (SI, Figure S7C), which was quite close to that of FP100 micelles (39.2 °C) (Figure 3B), indicating a similar thermoresponsiveness of the two micelles. Likewise, the size of FA-FP100 micelles was fully reversible during heating−cooling cycles between 25 and 55 °C (SI, Figure S7D). Besides, the opaque temperature and precipitated temperature of FA-FP100 micelles (SI, Figure S7E) were close to those of FP100 micelles as well (Figure 3E). Based on the above findings, FA-FP100 micelles were deemed to have an ideal thermoresponsive property such as FP100 micelles, probably due to the same F127/PLA ratio of them. As such, the DOX-loaded FA-FP100 micelles could keep stable under normothermia and

dx.doi.org/10.1021/am501422r | ACS Appl. Mater. Interfaces 2014, 6, 8549−8559

rapidly release drug at hyperthermia (SI, Figure S7F), and acidic pH further trigger drug release (SI, Figure S8).

Cytocompatibility Assay. To evaluate the cytocompatibility of FP100 and FA-FP100 blank micelles against mouse fibroblast NIH 3T3 cells and human cervix adenocarcinoma HeLa cells, Alarmar blue assay and live/dead staining were performed. The cells were incubated with different concentrations of the two blank micelles for 24 h. Alarmar blue assay demonstrated that the blank micelles had a high cell viability over 90% with 3T3 cells (SI, Figure S9A) in the concentration range 10−100 μg/mL. Besides, live/dead staining further demonstrated that the blank micelles were safe to 3T3 cells (SI, Figure S9B) up to the micellar concentration of 100 μg/mL. Considering HeLa cells would be used to evaluate the cytotoxicity of DOX-loaded micelles, a higher concentration of blank micelles were treated with HeLa cells in the cytocompatibility assay. The result indicated that the micelles had little toxicity to HeLa cells at concentrations up to 200 μg/mL, some of the cells were dead when treated with the micelles of 500 μg/mL (Figure 6). Thus, the polymeric micelles possess excellent cytocompatibility when the concentration is lower than 500 μg/mL.

Cellular Uptake and Intracellular Localization. To confirm the FR-mediated endocytosis of FA-decorated micelles, FR-positive human cervix adenocarcinoma HeLa cells and FR-negative human lung epithelial carcinoma A549 cells were incubated with free DOX, DOX-loaded FP100, and FA-FP100 micelles for fluorescence imaging investigations. No obvious fluorescence was observed from A549 cells after the incubation with either FP100 or FA-FP100 micelles (Supporting Information, Figure S10). In contrast, a strong red fluorescence was observed from HeLa cells incubated with FA-FP100 micelles, while HeLa cells incubated with FP100 micelles showed negligible nonspecific binding. It is worth mentioning that some of the FA-FP100 micelles are capable of escaping from the endo/lysosomes after 3 h and distributed in the nuclei (Figure 7).

Flow cytometry was carried out to quantitatively measure the cellular uptake of various DOX formulations. HeLa cells treated with DOX-loaded FA-FP100 micelles showed a prominent right shift upon cytometric analysis, suggesting greater cellular uptake of the FA-decorated micelles (Figure 8A). However, there was obvious variation in the mean fluorescence intensity (MFI) among different DOX formulations (Figure 8B). The MFI value of FA-FP100 group was 4.4-fold higher than FP100 group ($p < 0.05$) after treatment for 3 h, indicating that folate ligands could improve the target efficacy. The cellular uptake of free DOX was faster than that of FA-FP100 and FP100 micelles, which is mainly attributed to the passive diffusion mechanism of the internalization of this small molecule by cells.[42]

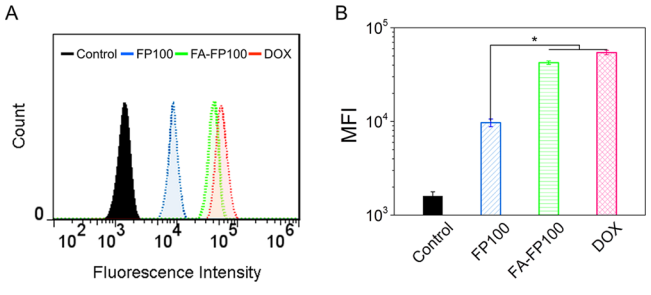

Figure 8. (A) Flow cytometry studies of HeLa cells incubated with various DOX formulations for 3 h. (B) Intracellular mean fluorescence intensity of HeLa cells treated with the three formulations. The results indicate significant differences on the fluorescence intensities of HeLa cells treated with or without folate-attached micelles: (*) $p < 0.05$.

Effect of Temperature on Cytotoxicity. The cytotoxicity of various DOX formulations was tested under short-term (1 h) low hyperthermia (40 °C) and normothermia (37 °C) conditions against HeLa cells. The live/dead staining images in Figure 9 showed that the cells treated with lower

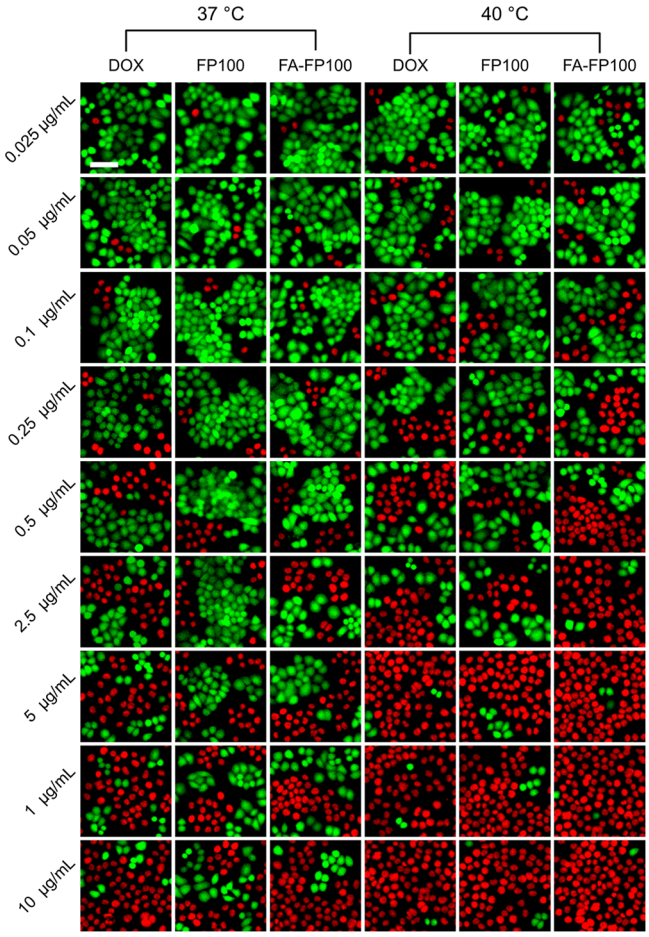

Figure 9. Fluorescence images showing the viability of HeLa cells following treatment with different concentrations of various DOX formulations at 37 and 40 °C. Green calcein fluorescence and red PI fluorescence indicating live and dead cells, respectively.

concentrations of DOX among the three groups possessed similar high viability upon the two temperatures, indicating that the low hyperthermia could not kill the cells within 1 h. Nevertheless, with the increasing of DOX concentrations, HeLa cells treated with various DOX formulations upon the low hyperthermia emerged varying degrees of enhancing necrosis compared with those under normothermia. The reason that the hyperthermia improves the cytotoxicity of DOX could be explained by several mechanisms, including increased drug levels and improved tissue oxygenation caused by increased perfusion, vascular permeability, and interstitial microconvection,[43] as well as the increased tumor cell sensitivity and DNA repair inhibition upon hyperthermia.[44] Moreover, the cytotoxicity of the thermoresponsive micelles affected by hyperthermia is more obvious than that of free DOX, indicating a rapid

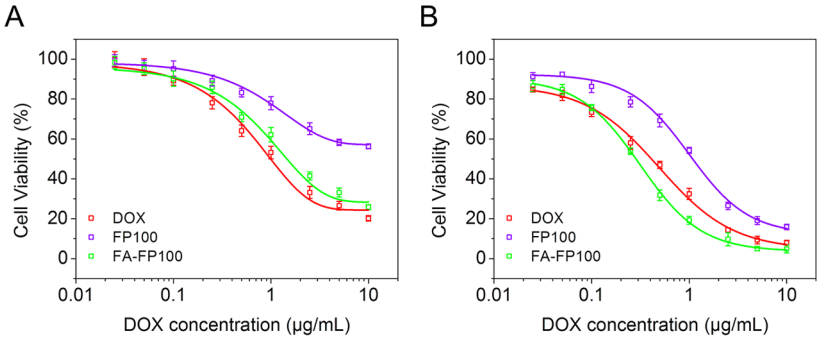

C

37 °C	DOX	FP100	FA-FP100	40 °C	DOX	FP100	FA-FP100
IC_{50}	0.99± 0.03		1.45 ± 0.03	IC_{50}	0.41 ± 0.02	1.08 ± 0.02	0.28 ± 0.02

Figure 10. Viability of HeLa cells after incubation with various DOX formulations at 37 °C (A) and 40 °C (B), and the table summarizes the IC_{50} (μg/mL) of various DOX formulations at 37 and 40 °C (C). Data are shown as mean ± SD (n = 4).

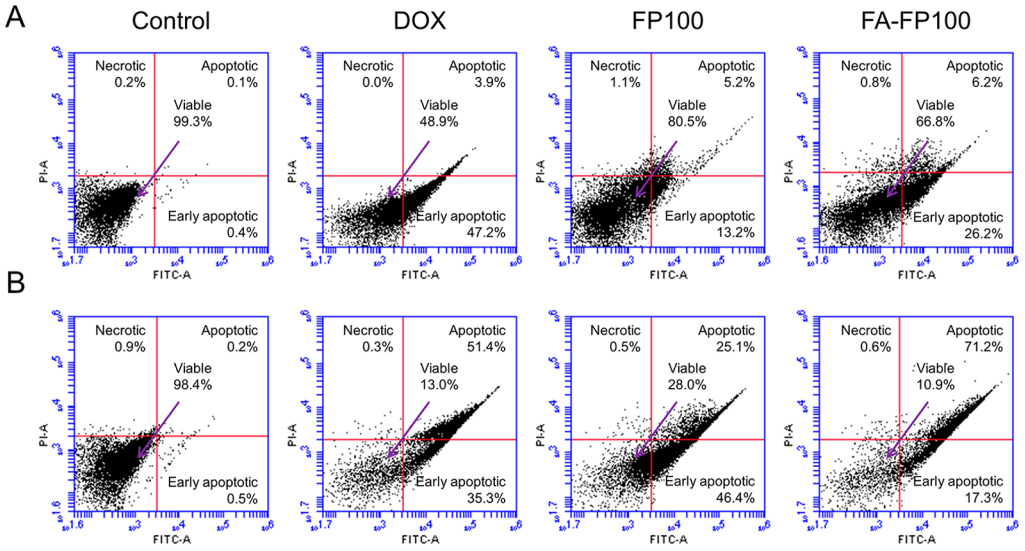

Figure 11. Flow cytometry analysis of necrosis in HeLa cells after treatment with PBS and various DOX formulations at 37 °C (A) and 40 °C (B).

release of cargo from these carriers at 40 °C, as discussed above (Figure 5 and SI Figure S8).

Figure 10 summarizes the results of cell viability and IC_{50} values after HeLa cells were incubated with free DOX, DOX-loaded FP100, and FA-FP100 micelles. Similar to the live/dead staining, Alarma blue assay quantitatively demonstrated that the DOX-loaded micelles were less cytotoxic at 37 °C, since the IC_{50} values of these micelles were higher than that of free DOX. This finding suggests that the amount of drug released from the thermoresponsive micelles at normothermia was not that much to cause a significant cell death. However, the IC_{50} values of micelles declined markedly when treating a short-term low hyperthermia, especially for the FA-FP100 micelles, which possessed a minimal IC_{50} value even lower than that of free DOX. In this case, the cell death was believed to arise from the prompt drug release of micelles under exogenous low hyperthermia and endogenous lysosomal acidic pH (SI, Figure S8D), and ultimately causing the death of cells. The targeted micelles induced more cells dead than FA-free micelles at both the temperatures, which was a result of more internalization by FR-mediated endocytosis.

Cell Apoptosis. To examine whether the thermoresponsive micelles modify cell apoptosis at different temperatures, Annexin V-FITC Apoptosis Detection kit was used to stain the HeLa cells after incubation with various DOX-formulations and the apoptotic cells were enumerated by flow cytometry. The cells with PBS treatment incubated at 40 °C for 1 h almost possessed the same viability in comparison with that upon 37 °C (control) (Figure 11), indicating that the low hyperthermia could not kill cells in a short period. In the contrary, compared to the treatment at 37 °C, the percentage of cells after incubation with DOX-loaded FP100 and FA-FP100 micelles at 40 °C undergoing apoptosis was significantly increased from 18.4 ± 1.2% and 32.4 ± 2.6% to 71.5 ± 4.9% and 88.5 ± 5.2%, respectively (Figure 11). Besides, the apoptotic cells in DOX group increased with temperature increasing as well, however, DOX group showed only 1.7-fold in apoptotic cells upon hyperthermia compared to normothermia, which is 3.9-fold in FP100 group and 2.7-fold in FA-FP100 group. The results based on the flow cytometry analysis were also in line with the cytotoxicity assay evaluated by Alarma blue assay (Figure 10) and live/dead staining (Figure 9). Compared to the thermoresponsive delivery systems previously developed for

dx.doi.org/10.1021/am501422r | ACS Appl. Mater. Interfaces 2014, 6, 8549−8559

mild hyperthermia-triggered drug release at 42−43 °C,[11,28,29] this micelle system displayed a rapid release of drug and significantly enhancing cytotoxicity against tumor cells under low hyperthermia (40 °C).

CONCLUSIONS

In summary, we have developed a FA-targeted and thermal-responsive micelle system with an ability of killing FR-overexpressed cancer cells under low hyperthermia. The micelles based on this F127-PLA copolymer with PLA segment having polymerization degree of 100 possessed a high thermoresponsiveness with an appropriate LCST value at 39.2 °C. These micelles could keep stable at normothermia (37 °C) while rapidly release encapsulated anticancer drug under low hyperthermia (40 °C). The polymeric micelles possessed excellent cytocompatibility, and the FA-decorated micelles could actively target folate receptor (FR)-overexpressed tumor cells. With low hyperthermia triggering, this drug delivery system could significantly amplify the induction of cancer cell apoptosis due to the rapid drug release in contrast to the treatment at normothermia. Therefore, this thermo-triggered system may have potential applicability in the area of controlling drug release on demand for effective cancer therapy.

ASSOCIATED CONTENT

Supporting Information

Synthesis route of FP copolymers, characterizations of copolymers and micelles, FTIR spectra, ^{1}H NMR spectra, CMC, cytocompatibility assay against 3T3 cells and cellular internalization by A549 cells. This material is available free of charge via the Internet at http://pubs.acs.org.

AUTHOR INFORMATION

Corresponding Author

*Email: shaobingzhou@swjtu.cn; shaobingzhou@hotmail.com.

Notes

The authors declare no competing financial interest.

ACKNOWLEDGMENTS

This work was partially supported by National Basic Research Program of China (973 Program, 2012CB933600), National Natural Science Foundation of China (Nos. 30970723, 51173150, 51373138), Research Fund for the Doctoral Program of Higher Education of China (20120184110029), and Construction Program for Innovative Research Team of University in Sichuan Province (14TD0050).

REFERENCES

(1) Peer, D.; Karp, J. M.; Hong, S.; Farokhzad, O. C.; Margalit, R.; Langer, R. Nanocarriers as an Emerging Platform for Cancer Therapy. *Nat. Nanotechnol.* **2007**, *2*, 751−760.

(2) Maeda, H.; Nakamura, H.; Fang, J. The EPR Effect for Macromolecular Drug Delivery to Solid Tumors: Improvement of Tumor Uptake, Lowering of Systemic Toxicity, and Distinct Tumor Imaging In Vivo. *Adv. Drug Delivery Rev.* **2012**, *65*, 71−79.

(3) Ulbrich, K.; Šubr, V. Polymeric Anticancer Drugs with pH-Controlled Activation. *Adv. Drug Delivery Rev.* **2004**, *56*, 1023−1050.

(4) Allen, T. M. Ligand-Targeted Therapeutics in Anticancer Therapy. *Nat. Rev. Cancer* **2002**, *2*, 750−763.

(5) Sudimack, J.; Lee, R. J. Targeted Drug Delivery via the Folate Receptor. *Adv. Drug Delivery Rev.* **2000**, *41*, 147−162.

(6) Dong, H. F.; Lei, J. P.; Ju, H. X.; Zhi, F.; Wang, H.; Guo, W. J.; Zhu, Z.; Yan, F. Target-Cell-Specific Delivery, Imaging, and Detection of Intracellular microRNA with a Multifunctional SnO_2 Nanoprobe. *Angew. Chem., Int. Ed.* **2012**, *51*, 4607−4612.

(7) Fan, N. C.; Cheng, F. Y.; Ho, J. A. A.; Yeh, C. S. Photocontrolled Targeted Drug Delivery: Photocaged Biologically Active Folic Acid as a Light-Responsive Tumor-Targeting Molecule. *Angew. Chem., Int. Ed.* **2012**, *51*, 8806−8810.

(8) Guo, X.; Shi, C. L.; Wang, J.; Di, S. B.; Zhou, S. B. pH-Triggered Intracellular Release from Actively Targeting Polymer Micelles. *Biomaterials* **2013**, *34*, 4544−4554.

(9) Ahmed, E.; Morton, S. W.; Hammond, P. T.; Swager, T. M. Fluorescent Multiblock π-Conjugated Polymer Nanoparticles for In Vivo Tumor Targeting. *Adv. Mater.* **2013**, *25*, 4504−4510.

(10) Mura, S.; Nicolas, J.; Couvreur, P. Stimuli-Responsive Nanocarriers for Drug Delivery. *Nat. Mater.* **2013**, *12*, 991−1003.

(11) Chung, M. F.; Chen, K. J.; Liang, H. F.; Liao, Z. X.; Chia, W. T.; Xia, Y.; Sung, H. W. A Liposomal System Capable of Generating CO_2 Bubbles to Induce Transient Cavitation, Lysosomal Rupturing, and Cell Necrosis. *Angew. Chem.* **2012**, *124*, 10236−10240.

(12) Zhou, S. B.; Fan, J.; Datta, S. S.; Guo, M.; Guo, X.; Weitz, D. A. Thermally Switched Release from Nnanoparticle Colloidosomes. *Adv. Funct. Mater.* **2013**, *23*, 5925−5929.

(13) Lee, J. H.; Chen, K. J.; Noh, S. H.; Garcia, M. A.; Wang, H.; Lin, W. Y.; Jeong, H.; Kong, B. J.; Stout, D. B.; Cheon, J. On-Demand Drug Release System for In Vivo Cancer Treatment through Self-assembled Magnetic Nanoparticles. *Angew. Chem.* **2013**, *125*, 4480−4484.

(14) Ruiz-Hernandez, E.; Baeza, A.; Vallet-Regí, M. Smart Drug Delivery through DNA/Magnetic Nanoparticle Gates. *ACS Nano* **2011**, *5*, 1259−1266.

(15) Czarnota, G. J.; Karshafian, R.; Burns, P. N.; Wong, S.; Al Mahrouki, A.; Lee, J. W.; Caissie, A.; Tran, W.; Kim, C.; Furukawa, M. Tumor Radiation Response Enhancement by Acoustical Stimulation of the Vasculature. *Proc. Natl. Acad. Sci. U.S.A.* **2012**, *109*, E2033−E2041.

(16) Feng, L. Z.; Yang, X. Z.; Shi, X. Z.; Tan, X. F.; Peng, R.; Wang, J.; Liu, Z. Polyethylene Glycol and Polyethylenimine Dual-Function-alized Nano-graphene Oxide for Photothermally Enhanced Gene Delivery. *Small* **2013**, *9*, 1989−1997.

(17) Yang, H.; Mao, H. J.; Wan, Z. H.; Zhu, A. J.; Guo, M.; Li, Y. L.; Li, X. M.; Wan, J. L.; Yang, X. L.; Shuai, X. T. Micelles Assembled with Carbocyanine Dyes for Theranostic Near-Infrared Fluorescent Cancer Imaging and Photothermal Therapy. *Biomaterials* **2013**, *34*, 9124−9133.

(18) Yan, Q.; Yuan, J. Y.; Cai, Z. N.; Xin, Y.; Kang, Y.; Yin, Y. W. Voltage-Responsive Vesicles Based on Orthogonal Assembly of Two Homopolymers. *J. Am. Chem. Soc.* **2010**, *132*, 9268−9270.

(19) Duan, X. Q.; Xiao, J. S.; Yin, Q.; Zhang, Z. W.; Yu, H. J.; Mao, S. R.; Li, Y. P. Smart pH-Sensitive and Temporal-Controlled Polymeric Micelles for Effective Combination Therapy of Doxorubicin and Disulfiram. *ACS Nano* **2013**, *7*, 5858−5869.

(20) Zeng, H. X.; Little, H. C.; Tiambeng, T. N.; Williams, G. A.; Guan, Z. B. Multifunctional Dendronized Peptide Polymer Platform for Safe and Effective siRNA Delivery. *J. Am. Chem. Soc.* **2013**, *135*, 4962−4965.

(21) Wang, J. Q.; Sun, X. R.; Mao, W. W.; Sun, W. L.; Tang, J. B.; Sui, M. H.; Shen, Y. Q.; Gu, Z. W. Tumor Redox Heterogeneity-Responsive Prodrug Nanocapsules for Cancer Chemotherapy. *Adv. Mater.* **2013**, *25*, 3670−3676.

(22) Chen, C. J.; Wang, J. C.; Zhao, E. Y.; Gao, L. Y.; Feng, Q.; Liu, X. Y.; Zhao, Z. X.; Ma, X. F.; Hou, W. J.; Zhang, L. R. Self-Assembly Cationic Nanoparticles Based on Cholesterol-Grafted Bioreducible Poly(amidoamine) for siRNA Delivery. *Biomaterials* **2013**, *34*, 5303−5316.

(23) Zhu, L.; Wang, T.; Perche, F.; Taigind, A.; Torchilin, V. P. Enhanced Anticancer Activity of Nanopreparation Containing an MMP2-Sensitive PEG-Drug Conjugate and Cell-Penetrating Moiety. *Proc. Natl. Acad. Sci. U.S.A.* **2013**, *110*, 17047−17052.

(24) Rao, J. Y.; Khan, A. Enzyme Sensitive Synthetic Polymer Micelles Based on the Azobenzene Motif. *J. Am. Chem. Soc.* **2013**, *135*, 14056−14059.

(25) Jayasundar, R.; Singh, V. P. In Vivo Temperature Measurements in Brain Tumors Using Proton MR Spectroscopy. *Neurol. India* **2002**, *50*, 436−439.
(26) Yahara, T.; Koga, T.; Yoshida, S.; Nakagawa, S.; Deguchi, H.; Shirouzu, K. Relationship between Microvessel Density and Thermographic Hot Areas in Breast Cancer. *Surg. Today* **2003**, *33*, 243−248.
(27) Issels, R. D. Hyperthermia Adds to Chemotherapy. *Eur. J. Cancer* **2008**, *44*, 2546−2554.
(28) Li, L.; ten Hagen, T. L. M.; Hossann, M.; Suss, R.; van Rhoon, G. C.; Eggermont, A. M. M.; Haemmerich, D.; Koning, G. A. Mild Hyperthermia Triggered Doxorubicin Release from Optimized Stealth Thermosensitive Liposomes Improves Intratumoral Drug Delivery and Efficacy. *J. Controlled Release* **2013**, *168*, 142−150.
(29) Dicheva, B. M.; ten Hagen, T. L. M.; Li, L.; Schipper, D.; Seynhaeve, A. L. B.; van Rhoon, G. C.; Eggermont, A. M. M.; Linder, L. H.; Koning, G. A. Cationic Thermosensitive Liposomes: A Novel Dual Targeted Heat-Triggered Drug Delivery Approach for Endothelial and Tumor Cells. *Nano Lett.* **2012**, *13*, 2324−2331.
(30) Lee, S. H.; Choi, S. H.; Kim, S. H.; Park, T. G. Thermally Sensitive Cationic Polymer Nanocapsules for Specific Cytosolic Delivery and Efficient Gene Silencing of siRNA: Swelling Induced Physical Disruption of Endosome by Cold Shock. *J. Controlled Release* **2008**, *125*, 25−32.
(31) Chen, S.; Li, Y.; Guo, C.; Wang, J.; Ma, J. H.; Liang, X. F.; Yang, L. R.; Liu, H. Z. Temperature-Responsive Magnetite/PEO-PPO-PEO Block Copolymer Nanoparticles for Controlled Drug Targeting Delivery. *Langmuir* **2007**, *23*, 12669−12676.
(32) Zhou, S. B.; Deng, X. M.; Yang, H. Biodegradable Poly(ε-caprolactone)−Poly(ethylene glycol) Block Copolymers: Characterization and Their Use as Drug Carriers for a Controlled Delivery System. *Biomaterials* **2003**, *24*, 3563−3570.
(33) Lu, H. F.; Lim, W. S.; Wang, J.; Tang, Z. Q.; Zhang, P. C.; Leong, K. W.; Chia, S. M.; Yu, H.; Mao, H. Q. Galactosylated PVDF Membrane Promotes Hepatocyte Attachment and Functional Maintenance. *Biomaterials* **2003**, *24*, 4893−4903.
(34) Batrakova, E. V.; Vinogradov, S. V.; Robinson, S. M.; Niehoff, M. L.; Banks, W. A.; Kabanov, A. V. Polypeptide Point Modifications with Fatty Acid and Amphiphilic Block Copolymers for Enhanced Brain Delivery. *Bioconjugate Chem.* **2005**, *16*, 793−802.
(35) Saul, J. M.; Annapragada, A.; Natarajan, J. V.; Bellamkonda, R. V. Controlled Targeting of Liposomal Doxorubicin via the Folate Receptor In Vitro. *J. Controlled Release* **2003**, *92*, 49−67.
(36) Lin, W. J.; Juang, L. W.; Lin, C. C. Stability and Release Performance of a Series of Pegylated Copolymeric Micelles. *Pharm. Res.* **2003**, *20*, 668−673.
(37) Ge, H. X.; Hu, Y.; Jiang, X. Q.; Cheng, D. M.; Yuan, Y. Y.; Bi, H.; Yang, C. Z. Preparation, Characterization, and Drug Release Behaviors of Drug Nimodipine-Loaded Poly(ε-caprolactone)−Poly(ethylene oxide)−Poly (ε-caprolactone) Amphiphilic Triblock Copolymer Micelles. *J. Pharm. Sci.* **2002**, *91*, 1463−1473.
(38) Huang, H. Y.; Hu, S. H.; Chian, C. S.; Chen, S. Y.; Lai, H. Y.; Chen, Y. Y. Self-Assembling PVA-F127 Thermosensitive Nanocarriers with Highly Sensitive Magnetically-Triggered Drug Release for Epilepsy Therapy In Vivo. *J. Mater. Chem.* **2012**, *22*, 8566−8573.
(39) Fleige, E.; Quadir, M. A.; Haag, R. Stimuli-Responsive Polymeric Nanocarriers for The Controlled Transport of Active Compounds: Concepts and Applications. *Adv. Drug Deliver. Rev.* **2012**, *64*, 866−884.
(40) Martin, G. R.; Jain, R. K. Noninvasive Measurement of Interstitial pH Profiles In Normal and Neoplastic Tissue Using Fluorescence Ratio Imaging Microscopy. *Cancer Res.* **1994**, *54*, 5670−5674.
(41) Hubbell, J. A. Enhancing Drug Function. *Science* **2003**, *300*, 595−596.
(42) Liang, X. J.; Wei, T.; Liu, J.; Ma, H. L.; Cheng, Q.; Huang, Y. Y.; Zhao, J.; Huo, S. D.; Xue, X. D.; Liang, Z. C. Functionalized Nanoscale Micelles Improve The Drug Delivery for Cancer In Vitro and In Vivo. *Nano Lett.* **2013**, *13*, 2528−2534.
(43) Song, C. W. Effect of Local Hyperthermia on Blood Flow and Microenvironment: A Review. *Cancer Res.* **1984**, *44*, 4721s−4730s.
(44) Krawczyk, P. M.; Eppink, B.; Essers, J.; Stap, J.; Rodermond, H.; Odijk, H.; Zelensky, A.; van Bree, C.; Stalpers, L. J.; Buist, M. R. Mild Hyperthermia Inhibits Homologous Recombination, Induces BRCA2 Degradation, and Sensitizes Cancer Cells to Poly(ADP-ribose) Polymerase-1 Inhibition. *Proc. Natl. Acad. Sci. U.S.A.* **2011**, *108*, 9851−9856.